Lab on a Chip

PAPER

Cite this: *Lab Chip*, 2025, **25**, 354

An intimal-lumen model in a microfluidic device: potential platform for atherosclerosis-related studies†

Fahima Akther,[ab] Dimple Sajin,[ac] Shehzahdi S. Moonshi,[ac] Jessica Pickett,[ac] Yuao Wu,[ac] Jun Zhang,[a] Nam-Trung Nguyen[ac] and Hang Thu Ta *[abc]

Received 14th October 2024,
Accepted 12th December 2024

DOI: 10.1039/d4lc00868e

rsc.li/loc

Atherosclerosis is a chronic inflammatory vascular disorder driven by factors such as endothelial dysfunction, hypertension, hyperlipidemia, and arterial calcification, and is considered a leading global cause of death. Existing atherosclerosis models have limitations due to the absence of an appropriate hemodynamic microenvironment *in vitro* and interspecies differences *in vivo*. Here, we develop a simple but robust microfluidic intimal-lumen model of early atherosclerosis using interconnected dual channels for studying monocyte transmigration and foam cell formation at an arterial shear rate. To the best of our knowledge, this is the first study that creates a physiologically relevant microenvironment under an arterial shear rate to modulate lipid-laden foam cells on a microfluidic platform. As a proof of concept, we use murine endothelial cells to develop a vascular lumen in one channel and collagen-embedded murine smooth muscle cells to mimic the subendothelial intimal layer in another channel. The model successfully triggers endothelial dysfunction upon TNF-α stimulation, initiating monocyte adhesion to the endothelial monolayer under the arterial shear rate. Unlike existing *in vitro* models, native low-density lipoprotein (LDL) is added in the culture media instead of ox-LDL to stimulate subendothelial lipid accumulation, thereby mimicking more accurate physiology. The subendothelial transmigration of adherent monocytes and subsequent foam cell formation is also achieved under flow conditions in the model. The model also investigates the inhibitory effect of aspirin in monocyte adhesion and transmigration. The model exhibits a significant dose-dependent reduction in monocyte adhesion and transmigration upon aspirin treatment, making it an excellent tool for drug testing.

1. Introduction

Atherosclerosis is caused by endothelial dysfunction, oxidative stress, hypercoagulability, and an elevated low-density lipoprotein (LDL) level.[1–6] Early pathogenesis of atherosclerosis starts with the formation of fatty streak by LDL accumulation in the intima, followed by enzymatic oxidation of LDL that provokes the infiltration of monocytes and T lymphocytes in the vascular intima.[7–9] Monocyte-to-macrophage differentiation causes the engulfment of the oxidised LDL that eventually converts into foam cells, a hallmark of the early stage of atherosclerosis.[10–13] Early detection is the prerequisite for the successful treatment of atherosclerosis. The complex disease mechanism makes early diagnosis difficult. In addition, researchers are also working on targeted drug delivery systems that can prevent specific biochemical interventions in early atherosclerosis pathogenicity.

The commonly used *in vitro* models for early atherosclerosis include chemotaxis-induced two-dimensional (2D) trans-well systems with pore sizes ranging from 3–8 μm.[14–20] Three-dimensional (3D) hydrogel-based coculture models have become popular due to their ability to establish cell–matrix interaction.[21] These models provide environments for studying biological mechanisms underlying the disease easily and inexpensively.[22] However, precision and model reproducibility with hemodynamic modulation remain a constant concern for these *in vitro* models. In laboratory set-up, a variety of animal models of atherosclerosis have been developed including mice,[23] rats,[24] rabbits,[25] and pig models.[26]

After *in vitro* validation, every newly developed drug needs to be tested through several rounds of animal testing before they can be tested on human. However, there are many

[a] *Queensland Micro- and Nanotechnology, Griffith University, Nathan, Queensland 4111, Australia. E-mail: h.ta@griffith.edu.au; Tel: +61 (7) 3735 5384; Web: https://hangta.group/; Web: https://experts.griffith.edu.au/27034-hang-ta*
[b] *Australian Institute for Bioengineering and Nanotechnology, The University of Queensland, St Lucia, Queensland 4072, Australia*
[c] *School of Environment and Science, Griffith University, Nathan, Queensland 4111, Australia*

† Electronic supplementary information (ESI) available. See DOI: https://doi.org/10.1039/d4lc00868e

barriers to animal testing, including ethical concerns as animal testing causes pain and suffering to sentient beings. Additionally, the majority of animal models often fail to replicate human-specific atherosclerosis due to interspecies differences in vascular physiology, immune responses, and lipid metabolism.[22,27] For example, developing plaques in mice models that differ significantly from those in humans.[24,28] Genetic modification such as apolipoprotein E (ApoE) knockout and low-density lipoprotein receptor (LDLR) knockout in mice, is often a prerequisite for developing atherosclerosis.[29] Furthermore, successful drug experiments in animals may be ineffective in humans because of genetic and phenotypic differences.[30] Thus, a high-efficiency, low-cost *in vitro* atherosclerosis model is still needed.

Microfluidic *in vitro* models overcome these limitations by using human-derived cells to capture patient-specific pathophysiology, providing precise control over microenvironmental factors such as shear stress and biochemical gradients, and enabling high-throughput testing, thereby offering a more physiologically relevant platform for studying atherosclerosis and evaluating therapies. While less impactful, developing microfluidic *in vitro* models using animal cells as platforms for validating and optimising therapeutics is also beneficial as they offer a promising solution to reduce the number of animals required for testing, addressing significant ethical concerns in biomedical research.

Till date, only a few studies used microfluidic platforms to study the pathophysiology of atherosclerosis.[22,31–35] Zheng *et al.*[32] developed a microfluidic model that mimicked physiological and atherosclerosis-prone hemodynamic conditions on a polydimethylsiloxane (PDMS) device. They combined mechanical (fluid shear stress and cyclic stretch) and biochemical conditions (hyperglycaemic and hyperlipidemic) to capture the endothelial responses in early atherosclerosis. The team proved their model's significance in determining probucol cytotoxicity, which was not detected in the Petri dish. Moreover, their model evaluated the anti-atherosclerosis efficiencies of platinum nanoparticles (Pt-NPs) by reducing oxidant exposure-induced cell death, which was in good agreement with the mouse model. Another study developed a tunable stenosis model to investigate the inflammatory cell–endothelial interaction in atherosclerosis.[36] The model created flow disturbances using different vessel stenosis and checked the influence of flow disturbance in monocyte recruitment. Shin *et al.*[37] replicated early atherosclerotic lesions by adjusting the vascular intimal stiffness using polyacrylamide gel with different concentrations along with extracellular matrix proteins (fibronectin and collagen) and checking endothelial integrity on a chip. They compared the cell migration and morphological changes in different stiffness with ECM coating. Fibronectin decreased endothelial integrity in the stiff polyacrylamide gel compared to collagen, suggesting the importance of intimal stiffness and matrix protein in endothelial dysfunction.

An early sign of atherosclerosis is the formation of foam cells in the subendothelial intimal space, resulting from the monocyte recruitment in the dysfunctional endothelial.[38] Limited studies have employed microfluidic platforms for monocyte transmigration or lipid-laden foam cell formation. Only one recent work focused on developing a stretchable model using a three-dimensional coculture system for forming foam cells in a microfluidic platform.[39] To mimic the biological environment of blood vessels, smooth muscle cells, endothelial cells, and monocytes were subjected to nonuniform strain through an elastic membrane embedded in the device. Foam cell formation was successfully induced in co-culture by treatment with low-density lipoprotein and stretching, with subsequent mRNA and protein expression changes. The device was also sensitive to atorvastatin and had significant dose-dependent inhibition in foam cell formation. However, this model only addressed the effects of stretch on foam cell formation and did not consider other critical factors, including physiological blood flow, vascular geometry, and humoral microenvironment, limiting its accuracy in mimicking *in vivo* relevance conditions.

Considering the current gap and the future scope, we aim to develop a microfluidic early-atherosclerosis model to induce *in vivo*-like monocyte transmigration and foam cell formation under a physiological shear rate. To our best knowledge, this is the first study where we successfully intervene in cell–cell and cell–matrix interaction and introduce continuous fluid flow to trigger *in vivo*-like foam cell formation. The two interconnected microchannels mimic the vessel lumen (top) and the subendothelial intimal layer (bottom). We incorporated hemodynamic modulation into our device by a peristaltic pump to generate a shear rate in the vessel lumen (top channel) and stimulated endothelial dysfunction by TNF-α treatment. We used native LDL to get the subendothelial diffusion and oxidation in the model instead of oxidised (ox)-LDL. Like *in vivo* models, this model initiates monocyte adhesion on inflamed endothelial, followed by monocyte transmigration in the subendothelial space and foam cell formation upon lipid accumulation under a physiological shear rate (Fig. 1). We also observed an inhibitory effect of aspirin in monocyte adhesion in the model. The initial adhesion of monocytes and ultimate foam cell formation was reduced in the aspirin-treated group, demonstrating the potential to use the developed microfluidic model as a drug testing tool in atherosclerosis treatment.

In this study, we employed murine cells as a proof of concept to validate the functionality of our device. The primary objective was to demonstrate the platform's ability to simulate early atherosclerotic conditions and to establish its utility for future studies. While murine cells were used in this initial phase, the device can be adapted for human-derived cells in subsequent experiments to better replicate human pathophysiology. This approach allows for the refinement of the model before transitioning to more human-physiologically relevant systems. Nevertheless, the model as it is in this study could be used for validating and optimizing therapeutics before proceeding to animal testing. This method minimizes the need for animal testing, effectively tackling important ethical issues in biomedical research.

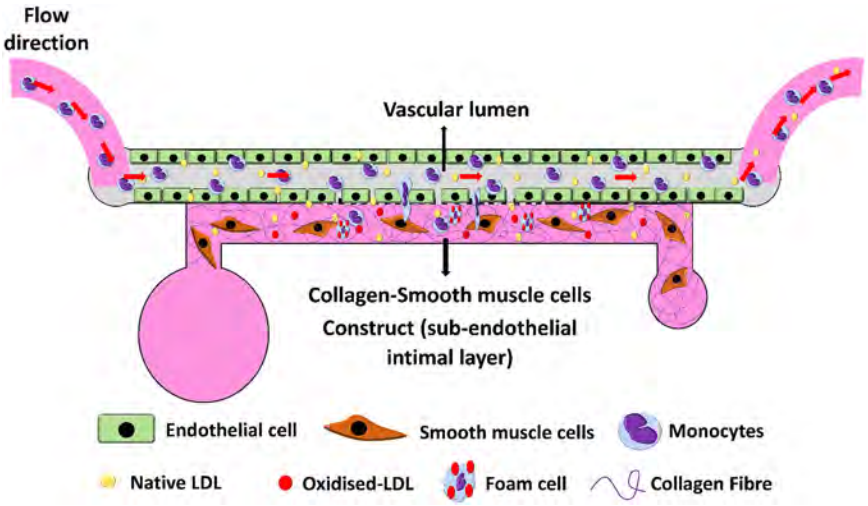

Fig. 1 Illustration of an early-atherosclerosis intimal-lumen model in a microfluidic device. Two interconnected microchannels provide a platform for cell–cell and cell–matrix interaction with hemodynamic modulation to achieve *in vivo*-like monocyte adhesion, transmigration, and foam cell formation under a physiological shear rate. Red arrows indicate the flow direction of monocytes.

2. Materials and methods

2.1. Microfluidic device design and fabrication

The device design was inspired by our previously developed site-specific atherothrombosis model[40,41] with some modifications in the channels' dimension. The device consists of dual-interconnected microchannels. The top channel mimicked the vascular lumen, while the bottom one represented the subendothelial intima. The dimensions of the channels are as follows: the top channel is 20 mm in length and 1 mm in width, and the bottom channel is 15 mm in length and 600 μm in width. The height of both channels is 100 μm. A 5 mm interconnected pillar spacings with a gap size of 6 μm formed the junction between the two channels (Fig. 2A).

Design parameters and patterns were defined using CleWin Software (WieWeb Software, The Netherlands) and printed on a transparent film. The technique used to fabricate the master mould is the dry etching, which removes the silicon material selectively and leaves the positive features. Then, the mould is coated with a thin layer of silane to make the surface hydrophobic. For PDMS device fabrication, the PDMS and curing agent were mixed at a ratio of 10 : 1 (Sylgard 184 Silicone Elastomer, Dow Corning, Midland, MI) and then degassed in a desiccator to remove air bubbles. The mixture was poured on the master mould and incubated for at least 2 h at 75 °C for PDMS solidification. The PDMS slab with embedded channels was peeled off from the silicon master mould and inlet and outlet holes in the top channel was punched using a 1.2 mm tip. The bottom channel's inlet was similar to the top channel, while a 10 mm tip was used to punch a media reservoir in the outlet hole. The PDMS slabs and the glass slides/coverslips were washed with isopropyl alcohol and water, air-dried, and kept in the oven (75 °C) for 2 min for complete drying, followed by plasma treatment (PDC-002, Harrick Plasma, Ossining, NY) at 1.4–1.8 torr for 2 min and bonded together. Fig. 2B shows the fabricated device with a scale and red dye for visualization of the microchannels. Fig. 2C is a schematic diagram of the experiment setup of our device.

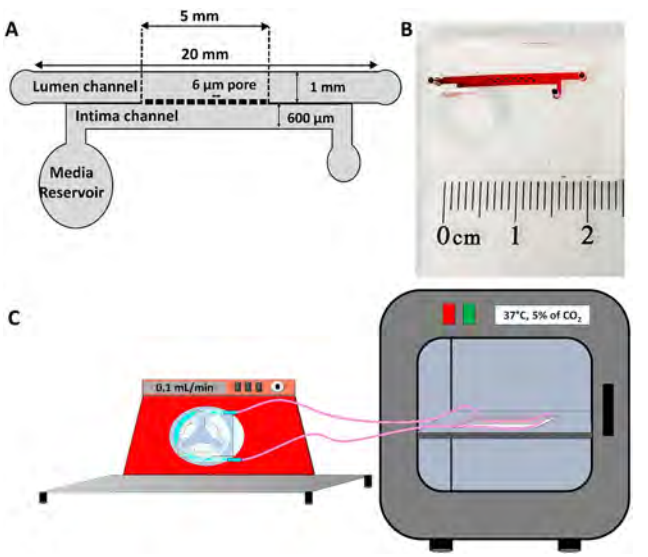

Fig. 2 A device with dual interconnected microchannels representing the early-atherosclerosis intimal-lumen model. (A) A schematic diagram of a microfluidic device with dual interlinked channels. The top channel mimicked a vascular lumen, whereas the bottom one represented the subendothelial intimal layer. (B) Image of the actual model after PDMS casting. A scale was placed to show the size of the device. The red dye was infused to facilitate clear visualisation of the microchannel. The dotted line indicates the porous junction region. (C) Schematic diagram of the experimental set-up of the microfluidic device.

In our study, we used a straight microfluidic channel. Due to the small dimension and low Reynold number (3.14) (ESI,† section S1), the flow is laminar in our device. In a rectangular channel, laminar flow typically establishes a parabolic velocity profile, with the highest velocities occurring at the center and diminishing to zero at the walls, by the no-slip boundary condition.

2.2. Cell culture and maintenance

We used SVEC4-10 (a murine endothelial cell line), MOVAS (a murine aortic smooth muscle cell), and RAW 264.7 (murine monocytes/macrophage-like cells) from ATCC, Rockville, MD. The cells were grown in DMEM (Dulbecco's modified Eagle medium) low glucose medium supplemented with 100 IU ml^{-1} of penicillin G, 100 μg ml^{-1} streptomycin, and 10% (v/v) FBS, at 37 °C in a humidified atmosphere, with 5% of CO_2. SVEC-10 and MOVAS were used within passage number 5–8. RAW 264.7 cells were used within passages 18–24.

2.3. Subendothelial intimal layer development in the bottom channel

Atherosclerosis subendothelial intimal layer consists of vascular smooth muscle cells (VSMCs) and the extracellular matrix (ECM).[42,43] This study used rat tail collagen (R&D biosystem, cat. no. 3443-100-01), a predominant ECM protein in the intima,[44] and MOVAS to mimic the subendothelial intimal layer. Due to the small dimension of the bottom channel, only approximately 5 μL of hydrogel precursor solution was needed to fill the channel. We used collagen concentrations ranging from 3–4 mg mL^{-1} with embedded MOVAS to determine the appropriate collagen concentration to form an intimal layer. Following the manufacturer's protocol, three different collagen concentrations of 3, 3.5, and 4 mg mL^{-1} hydrogel precursor solutions were prepared. To prepare 100 μL of 3 mg mL^{-1} neutralised collagen hydrogel precursor solution, 10 μL of 10× low glucose DMEM media (without FBS and antibiotics) was taken into a 1.5 mL vial, and then 60 μL of collagen stock solution (5 mg mL^{-1}) was added, followed by adding 3 μL sterile NaOH (1 M) to neutralise the solution. A 5 μL MOVAS suspension at a concentration of 2 million per 100 μL was added to the neutralised collagen solution and adjusted the remaining volume with deionised water. The final MOVAS concentration in the collagen solution was 100 000 cells per 100 μL. We infused 5 μL collagen-MOVAS suspension in the bottom channel of the device by pipetting and incubating it for 1 h (5% CO_2, 37 °C) for gel maturation. Each device contained 5000 MOVAS embedded in collagen in the bottom channel to mimic the subendothelial intimal layer. To prepare 3.5 and 4 mg mL^{-1} collagen-MOVAS suspension, we kept the MOVAS concentration similar to 3 mg mL^{-1} but adjusted the volume of the collagen stock to 70 and 80 μL, and also adjusted the volume of 1 M NaOH to 3.5 and 4 μL, respectively for neutralisation. The remaining volume was adjusted by deionised water. The MOVAS-collagen construct was grown for 5 days, and LIVE/DEAD™ Viability/Cytotoxicity Kit (Invitrogen™, cat. no. L3224) was used to check the live and dead cells in the collagen construct. This assay kit offered two-colour visualisation of LIVE/DEAD populations based on membrane integrity and esterase activity. Plasma membrane integrity was determined by ethidium homodimer (EthD)-1, which entered cells with a compromised plasma membrane to bind DNA and emit a red fluorescence, indicating dead cells. Calcein AM converted to a green fluorescence after interaction with intracellular esterase and identified the live cells. The images were taken at a 494 nm excitation filter for calcein AM and a 517 nm excitation filter for EthD-1 using an inverted microscope (CKX53, Olympus) mounted with a digital camera (DP74, Olympus). Three different microscopic field views at 4× magnification of the bottom channel were taken to record the fluorescence intensity throughout the channel. Data (n = 3) was analysed by image processing software Fiji ImageJ (Java 1.8.0_172).

2.4. Flow rate calculation for mimicking physiological shear rate in the top channel

The average recorded physiological shear rate of the medium artery is within the range of 500–2500 s^{-1}, while most *in vitro* studies used 1000 s^{-1} to mimic the hemodynamic physiology in the microfluidic channel.[45] In the present study, we introduced a 1000 s^{-1} shear rate in the top channel using a programmable peristaltic pump (model: NE-9000, ALA Scientific) to replicate the arterial shear rate (Fig. 2C). The flow rate was calculated as follows.

To convert the arterial shear rate (1000 s^{-1}) into flow rate, the relation between shear stress, shear rate and viscosity is:

$$\tau = \eta \times \gamma \quad (1)$$

where, τ is shear stress, η is fluid viscosity (Pa s) and γ is shear rate (s^{-1}).

The dynamic viscosity of DMEM containing 10% FBS (η) = 0.964×10^{-3} Pa s (ref. 46 and 47) = 0.964×10^{-2} dyn s cm^{-2}.

The shear stress was expressed as the following eqn (1)–(4)

$$\tau = \frac{6\eta Q}{h^2 w} \quad (2)$$

Then

$$\gamma = \frac{6Q}{h^2 w} \quad (3)$$

Finally, we can get the expression of flow rate Q:

$$Q = \gamma h^2 w/6 \quad (4)$$

where, γ = 1000 s^{-1}, h = height of the channel = 100 μm, w = width of the channel = 1 mm. Therefore, Q = 100 μL min^{-1}.

2.5. Endothelial cell attachment and development of vascular lumen in the top channel

The surface of the PDMS device is hydrophobic and requires modification for cell attachment.[48] Our study used bovine skin collagen (Sigma-Aldrich, cat. no. C4243) as a coating material to improve PDMS hydrophilicity and surface roughness for cell attachment. Briefly, 10 μL of collagen stock was mixed with 90 μL of plain low-glucose DMEM media (without FBS and antibiotics) to get the final collagen concentration at 333 μg mL^{-1}. A 10 μL coating solution was infused through the top channel and incubated for an hour (5% CO_2, 37 °C). The solution was removed from the channel and washed twice with PBS to remove the excess collagen. SVEC-10 was cultured in a flask and trypsinised when confluent. A suspension of SVEC-10 was prepared at a concentration of 30 million per mL and infused through the top channel. Approximately 10 μL cell suspension was required to cover the whole channel. We used concentrated cell suspension to maximise cell adhesion to the PDMS surface because only a few cells could attach. The device was then incubated on a shaking incubator at 37 °C and 100 rpm for an hour. Next, the device was moved to the cell incubator and incubated for an hour upside down to facilitate cell attachment on the upper wall of the top channel. Finally, we flipped the device back and incubated it in static conditions for another 3 h for better cell attachment in all walls of the top channel. We filled the media reservoir with fresh media during the last 3 h incubation to prevent hydrogel drying. Endothelial cells attached and spread throughout the top channel after 5 h of incubation. Finally, we introduced flow using a peristaltic pump at a 40 μL min^{-1} rate equivalent to a 400 s^{-1} shear rate and grew the cells overnight. Subsequently, we increased the flow rate to 100 μL min^{-1} (~1000 s^{-1} shear rate) to grow the cells at an arterial shear rate until they reached confluency. The reservoir was re-filled with fresh media every 24 h.

2.6. Staining for confirming endothelial integrity

Once the SVEC-10 reached confluency and covered the top channel completely, the media was removed and washed with PBS, then 4% PFA was added to the top channel and the reservoir to fix the cells. The device was incubated for an hour at room temperature (RT) in static conditions to allow the complete fixation of the whole system. The device can be stored at 4 °C or used immediately. The PFA was removed, and the top channel was washed with PBS thrice. The SVEC-10 cells in the top channel were permeabilised using 0.1% Triton-X 100 and incubated 20 min at RT. The top channel was washed with PBS thrice and then blocked with 1% BSA (bovine serum albumin) in PBS for an hour at RT. Finally, the cells were stained with CellMask™ plasma membrane stains (Invitrogen™, cat. no. C37608) and Hoechst 33342 (Invitrogen™, cat. no. 62249) for nucleus staining for 20 min at RT and then washed with PBS twice before imaging. The imaging was taken using the above-mentioned inverted microscope and imaging system. The Z-stack images were taken using a confocal microscope (Olympus FV3000RS NIR). The images were processed using Fiji ImageJ, and the 3D image reconstruction was achieved by Olympus FLUOVIEW (FV31S-SW) software.

2.7. Endothelial barrier integrity measurements

The integrity of the endothelial monolayer was assessed by measuring the transendothelial electrical resistance (TEER). TEER measurements were performed using a voltage-ohm meter (87V Industrial Multimeter, Fluke Corporation, Everett, WA) connected to Ag/AgCl electrode wires (0.008″ in diameter; A-M Systems, Inc., Sequim, WA). To ensure accurate TEER readings (R_{TISSUE}), a baseline resistance (R_{Blank}) was measured in the absence of cells and subtracted from the total resistance measured for the endothelial monolayer (R_{Total}), as outlined in eqn (5). The corrected resistance (R_{TISSUE}) was then multiplied by the total surface area of the cell culture on the PDMS membrane, as described in eqn (6).

$$R_{TISSUE}\ (\Omega) = (R_{Total} - R_{Blank}) \quad (5)$$

TEER values are typically represented ($TEER_{REPORTED}$) in units of Ω cm^2 and calculated as:

$$TEER_{REPORTED} = R_{TISSUE}\ (\Omega) \times M_{AREA}\ (cm^2) \quad (6)$$

2.8. Low-density lipoprotein isolation from serum

Whole blood was obtained from Australian Red Cross Blood Service under a human ethics approved by Griffith University Human Research Ethics Committee (2021/598). The low-density lipoprotein (LDL) was separated from whole blood serum using potassium bromide density gradient ultracentrifugation, followed by slightly modified previous protocols.[49] Whole blood sample was collected from the Australian Red Cross Blood Service and centrifuged for 10 min at 2000 × *g*. The supernatant of platelet-rich plasma was collected. Additional centrifugation at 10 000 × *g* for 30 min was performed to remove the platelets and the supernatant was collected. Plasma solvent density was adjusted by potassium bromide (KBr) to achieve 1.063 g mL^{-1}, using the following formula:

$$\text{Amount of KBr added } (g) = \text{Volume of Plasma (mL)} \times 0.0834$$

The density-adjusted plasma solution was added to a 38.5 mL open-top thin wall ultra-clear polycarbonate tube (Beckman Coulter, cat. no. 344058). The plasma was centrifuged for 24 h at 40 000 rpm at 4 °C, using a 70 Ti rotor (Optima XPN-90 Ultracentrifuge). After 24 h of centrifugation, the supernatants were removed, and the LDL-rich layer separated by density gradient was collected.

LDL was then dialysed against PBS (pH 7.4) for 24 h, with PBS changed every 6 h. LDL was stored at 4 °C and used within 2 weeks. The protein concentration was checked by standard BCA (bicinchoninic acid) protein assay following manufacturer instructions. Finally, the isolation of LDL was confirmed by SDS-PAGE electrophoresis (Fig. S1†). Moreover, oxidised low-density lipoprotein (ox-LDL) was quantified using a Lipid Peroxidation (MDA) Assay Kit (ab118970) according to the manufacturer's protocol (ESI,† section S2). No oxidation was detected after 2 weeks of LDL storage at 4 °C.

2.9. Initiating monocyte transmigration and foam cell formation in microfluidic platform

SVEC-10 cells formed a confluent monolayer on the top channel after two days of incubation under an arterial shear rate and mimicked the vessel lumen with tight endothelial junctions. The top channel was treated with 10 ng mL^{-1} TNF-α and 25 μg mL^{-1} LDL for 8 h under the arterial shear rate (~1000 s^{-1} shear rate) using a peristaltic pump to induce endothelial dysfunction. The cell viability/metabolic activity was checked to select the optimal treatment time for TNF-α. SVEC-10 and RAW 264.7 cells maintained good cell viability in all concentrations up to 24 h. However, a significant reduction in the MOVAS viability was observed after 8 h of treatment in all TNF-α except 25 pg mL^{-1} (Fig. S2†). Monocytes (RAW 264.7 cells) were cultured in a Petri dish, tagged with nuclear staining dye (Hoechst 33342) for 20 min and washed with PBS thrice. The cells were detached with a cold medium and counted using a hemocytometer. The monocyte suspension was made at 500 000 cells per mL to infuse through the top channel. A syringe pump infused the monocyte suspension through the top channel for an hour at the arterial shear rate of 1000 s^{-1}. The images were taken at 15 min intervals to record monocyte adhesion on the SVEC-10 monolayer. The cells were counted using the automated particle counting option in the Fiji ImageJ software. A control group without TNF-α stimulation but LDL treatment was run to compare monocyte adhesion and subsequent transmigration to those with TNF-α stimulation. After 1 h, the device was topped with fresh media and incubated under flow conditions (1000 s^{-1}) for another 24 h to trigger subendothelial monocyte transmigration and lipid-laden foam cell formation.

2.10. Preparation of oil-red-o and Giemsa dye

The stock solution concentration of oil-red-o was 0.5% in 100% isopropanol (Sigma-Aldrich, cat. no. O1391). The working solution was prepared with a 6 : 4 ratio of oil-red-o stock solution and water. The solution was mixed properly and incubated for 10 min at room temperature. The solution was then filtered using a syringe filter with a filter pore size of 0.22 μm. The working solution must be used within 1 h of preparation for better staining.

Giemsa stock solution was prepared following the world health organisation standard protocol. Briefly, to make 500 mL Giemsa stock solution, 3.8 g Giemsa powder (Sigma-Aldrich, G5637) was measured and poured into a clean glass bottle. 100 mL absolute methanol was added to the bottle and mixed at a circular motion for 2–3 min. Then, 250 mL glycerol was added to the mixture and shaken for another 3–5 min. Finally, the remaining 150 mL of absolute methanol was poured into the mixture and mixed properly. The stock solution was stored in a dark and cool place. Shaking the stock solution for 2–3 min at least six times daily for the first 7 days of incubation is important. The stock solution was incubated for at least 6 weeks before use. A working solution was made by diluting the stock solution 20 times in water. The working solution was used within 15 min after preparation.

2.11. Quantification of monocyte transmigration and foam cell formation in microfluidic platform

After 24 h incubation of monocytes under the arterial shear rate, the SVEC-10 monolayer from the top channel was trypsinised and detached completely. Collagenase-D was used to digest the subendothelial intimal layer and collect the transmigrated monocytes/foam cells. A 2.5 mg mL^{-1} collagenase-D solution in PBS was infused through the top channel (10 μL) and added in the media reservoir. The device containing collagenase D was incubated at 37 °C for an hour to completely digest the collagen hydrogel from the bottom channel. The collagenase D solution was collected from the device, including the solution from the reservoir, and collected in a vial. The device was washed with PBS thrice and the washing solution was collected in the same vial. The mixture was centrifuged at 300 × *g* for 5 min, the supernatant was discarded, and the cell pellet was resuspended in 10 μL fresh media. This 10 μL suspension was pipetted on a glass slide to make a thin smear for cell counting. The slides for all samples were air-dried for 20 min at RT and blow-dried with a dryer for 10 s. We then fixed the slides with 4% PFA for 15 minutes and 78% methanol for another 15 min. A 500 μL of oil-red-o working solution was added to each slide and incubated for 15 min for lipid staining. The slides were washed with 78% methanol twice, then counterstained with a working solution of Giemsa for 1 min for monocyte staining and washed with distilled water. The previously mentioned microscope and imaging software were used to take the brightfield images. Foam cells were identified by the accumulation of lipid droplets in the cell cytoplasm. The foam cells appeared with light pink/purple cytoplasm and red/orange lipid droplets with a foamy morphology. The non-foamy monocytes were determined by distinct deep purple/bluish purple cytoplasm without any lipid accumulation. The total transmigrated monocytes/foam cells were counted manually under a microscope. The foam cell percentage in the transmigrated cells was calculated using the following equation.

$$\text{Foam cell in total transmigrated cell (\%)} = \frac{\text{Total number of foam cells in the collagen construct}}{\text{Total number of transmigrated monocytes and foam cells}} \times 100\%$$

We also stained the collagen construct into the bottom channel with Giemsa dye for visual confirmation of monocyte transmigration into the subendothelial layer. The cells were detached from the top channel and the bottom collagen construct was fixed with 4% PFA at RT for an hour. The model was then incubated for 15 min with 78% methanol, followed by another 30 min incubation with Giemsa dye at RT. The cells were observed under the inverted microscope mentioned above. The microscope's focus was adjusted to scroll down the intimal construct and images were taken to confirm the cell transmigration. Monocytes appeared with dark purple/bluish purple cytoplasm in the collagen construct.

2.12. Inhibitory effect of aspirin in monocyte adhesion and transmigration

All steps were done under arterial shear rate (~1000 s^{-1}). The SVEC-10 cells were grown in the top channel until they formed a confluent monolayer. The SVEC-10 monolayer was then treated with 50 and 100 μM aspirin for 4 h. Meanwhile, after aspirin treatment, TNF-α and LDL were added to the same media containing aspirin and treated for another 8 h. So, the total treatment time for aspirin was 12 h and the time for TNF-α and LDL was 8 h. The final concentration of TNF-α and LDL in the media was 10 ng mL^{-1} and 25 μg mL^{-1}, respectively. Monocyte adhesion and transmigration studies were done according to the procedures mentioned above. Positive controls were prepared without aspirin but treated with TNF-α and LDL for 8 h. A negative control was prepared without aspirin and TNF-α, but the model was treated with LDL for 8 h. Monocytes (500 000 cells per mL) were infused through the top channel for an hour. The images were taken at 15 min intervals using an inverted microscope to check the initial monocyte adhesion on the SVEC-10 monolayer. After 1 h, the device was topped with fresh media and incubated for another 24 h to trigger subendothelial monocyte transmigration and lipid-laden foam

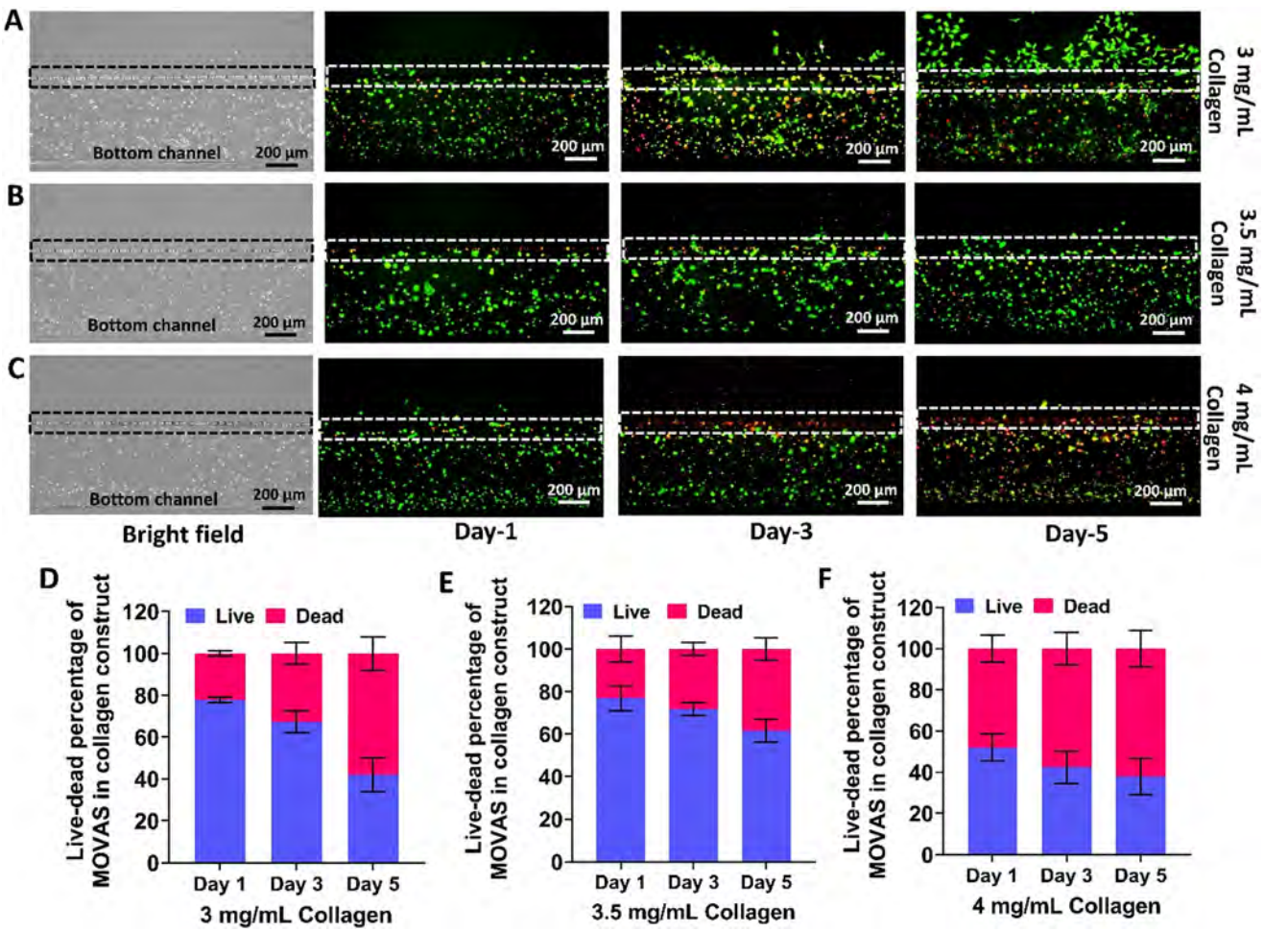

Fig. 3 Detection of live and dead MOVAS cells in the collagen construct. The cells were stained with a LIVE/DEAD™ Viability/Cytotoxicity Kit. Live cells appeared green, while dead cells appeared red in the fluorescence images. Live/dead assay of MOVAS embedded in 3 mg mL^{-1} (A), 3.5 mg mL^{-1} (B), and 4 mg mL^{-1} (C) collagen construct. The brightfield images were taken on day-1. Fluorescence images were taken at a 494 nm excitation filter for calcein AM and a 517 nm excitation filter for EthD-1. Live-dead percentage of MOVAS at days 1, 3, and 5 in 3 mg mL^{-1} (D), 3.5 mg mL^{-1} (E), and 4 mg mL^{-1} (F) collagen construct. Values are mean ± SD, n = 3. Dotted lines highlighted the porous junction region.

cell formation. The total transmigrated cells and the percentage of foam cells in the total transmigrated cells in different groups were counted as the prior-mentioned method. The number of the initial adherent monocytes was counted using the automated particle counting option in the Fiji ImageJ software.

2.13. Statistics analysis

Data representation was mean ± standard deviation (SD) of three independent experiments. *T*-Test and one-way ANOVA were used to analyse the significant differences. A *p*-value of ≤ 0.05 was considered significant. Graphs were plotted using GraphPad Prism 9.

3. Results

3.1. Subendothelial intimal layer development in the bottom channel

We mimicked early atherosclerosis intimal layer with rat tail collagen and murine smooth muscle cells. Collagen was used in different concentrations to embed MOVAS and check the cell in the collagen construct. MOVAS showed rapid growth with elongated morphology in collagen construct with 3 mg mL^{-1} concentration. However, this concentration was not stiff enough to hold the MOVAS within the hydrogel construct. MOVAS migrated to the top channel *via* the porous junction, covering the top channel gradually (Fig. 3A). The fluorescence images clearly showed the migrated MOVAS in the top channel and covered the top channel at 5 days of incubation. Many dead cells (red) were also noticed on days 3 and 5. In collagen constructs at a concentration of 3.5 mg mL^{-1}, MOVAS showed a good blend of rounded and elongated morphology. Fluorescence images showed more live cells (green) than dead cells (red) in 5 days of incubation. The number of migrated MOVAS to the top channel was minimal (Fig. 3B). On the other hand, MOVAS in the collagen construct at 4 mg mL^{-1} mainly showed rounded morphology, and a significant number of dead cells (red) was observed in the fluorescence image after 5 days of incubation (Fig. 3C). Since the hydrogel was stiff due to its higher collagen concentration, minimal migration of MOVAS was observed. The percentage of the live and dead cells was calculated in three collagen concentrations. Approximately 80% viable cells were detected in the 3 mg mL^{-1} collagen construct on day 1. However, the number of viable cells reduced gradually and only ~40% viable cell was detected in 5 days of incubation (Fig. 3D). MOVAS maintained good viability (~75%) in 3.5 mg mL^{-1} collagen construct for up to 3 days, while the viability reduced slightly on day 5 (Fig. 3E). On the other hand, the collagen construct with 4 mg mL^{-1} concentration showed the lowest cell viability from day 1. Only ~50% of cells were viable at day 1 and reduced to ~35% at day 5 (Fig. 3F). Among the three concentrations, the 3.5 mg mL^{-1} collagen construct maintained higher MOVAS viability with less cell migration towards the top channel, making the concentration suitable for forming the intimal layer. It is noteworthy that in the top channel, no fluid flow was applied, and endothelial cells were absent.

3.2. Vascular lumen development in the top channel

The SVEC-10 cells attached within 5 h of static incubation in the collagen-coated top channel. The cell adhesion was strong enough to sustain the initial flow at 40 μL min^{-1}. A confluent monolayer of the SVEC-10 cells, covering all side walls, was achieved after 48 h of incubation under an arterial shear rate of 1000 s^{-1}. In this device, endothelial cells grew throughout the top channel and a MOVAS-collagen construct formed in the bottom channel, confirming the development of an atherosclerosis intimal-lumen model (Fig. 4A). Plasma membrane and nucleus staining further confirmed the confluent monolayer of the SVEC-10 cells in the top channel (Fig. 4B).

We further observed the device under a confocal microscope to confirm the endothelial integrity on the interconnecting porous junction between two channels. Z-Stack images were taken to check the endothelial barrier over the porous junction. The top view of the side wall containing the porous junction showed a confluent integral endothelial monolayer over the pores. The green plasma membrane staining confirmed a compact inter-junction between the endothelial cells, and the merged images clearly showed the endothelial barrier over the porous junction area (Fig. 5A). The 3D-reconstructed images proved the endothelial attachment on all walls (top, bottom and side wall containing the porous junction) and exhibited a hollow lumen-like structure in the top channel (Fig. 5B and C). Moreover, the 3D-reconstructed images also showed a compact endothelial barrier on the porous junction. The plasma membrane and nucleus staining revealed a distinct wall-like barrier on the porous junction in the images of the side view (Fig. 5B) and the front view (Fig. 5C), confirming a tight endothelial barrier in that section.

Furthermore, we observed a steady increase in TEER over 5 days. We measured the TEER value to assess endothelial integrity both in static and flow conditions and observed a steady increase over time. However, the value did not significantly increase after 72 hours of incubation (Fig. 5D) in static conditions. The TEER value rose substantially when cells were grown under arterial shear rate, showing a steady increase after 5 days of incubation under flow conditions. This indicates uniform endothelial monolayer formation and consistent sensitivity distribution, as evidenced by the progressively higher TEER values (Fig. 5E). Notably, treatment with 10 ng mL^{-1} TNF-α or 25 μg mL^{-1} LDL for 24 h (commencing at 72 h time-point) resulted in a significant decrease in TEER (at 96 h time-point), reflecting disruption of the monolayer's integrity (Fig. 5F and G). The TNF-α-treated monolayer exhibited a more pronounced reduction in TEER (1.066×10^5 Ω) (Fig. 5E) compared to the LDL-treated group (7.834×10^4 Ω) (Fig. 5E), highlighting the greater impact of TNF-α on endothelial barrier function.

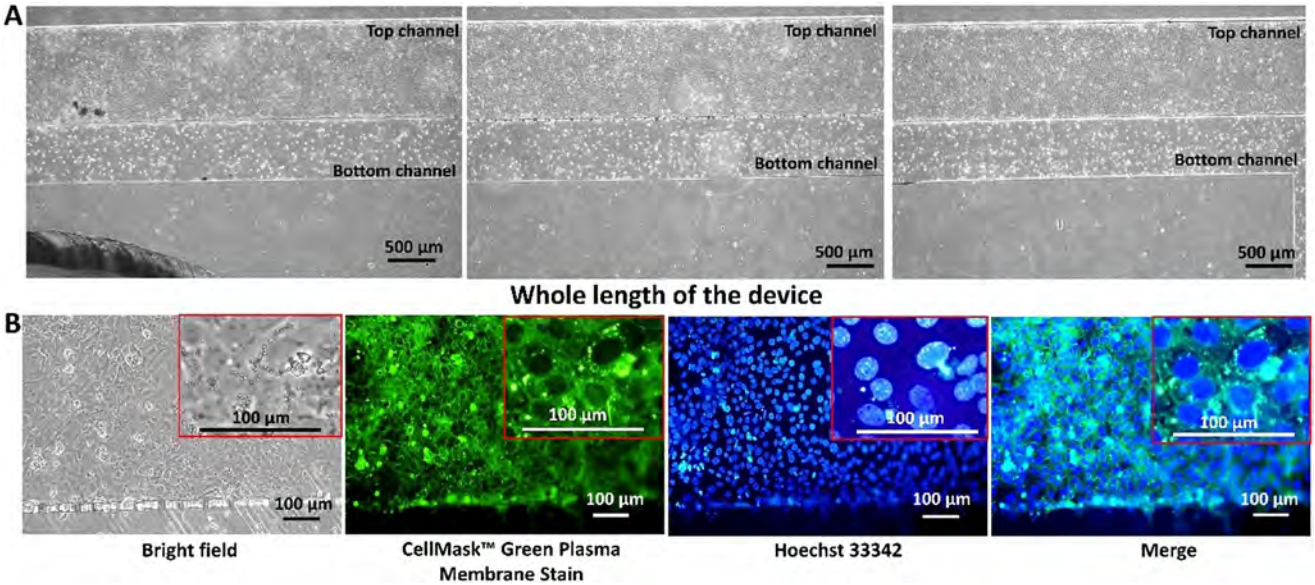

Fig. 4 An intimal-lumen model in a microfluidic platform. (A) Coculture formation of SVEC-10 and MOVAS in the dual-interconnected channels. The bottom channel contained collagen-embedded MOVAS, mimicking subendothelial intima, and the top channel was covered with endothelial monolayer, representing vessel lumen. (B) Confirmation of SVEC-10 cells monolayer formation on the top channel. Plasma membrane (green), nucleus (blue) staining, and the merged image confirmed a confluent monolayer of SVEC-10 cells on the top channel.

3.3. Monocyte transmigration and foam cell formation in the intimal-lumen model

Our study focused on developing an *in vivo*-like model for monocyte transmigration and foam cell formation. The first step was to test monocyte adhesion to the SVEC-10 monolayer in the top channel, which mimicked the vessel lumen. The atherosclerosis intimal-lumen model was treated with TNF-α to trigger endothelial dysfunction under an arterial shear rate. The cells were also treated with native LDL at a physiological range (25 μg mL^{-1}) to initiate LDL deposition in the intimal layer, eventually triggering foam cell formation. The monocytes were infused at a shear rate of 1000 s^{-1} for an hour. The cell concentration used in this experiment was 500 000 cells per mL, within range of the physiological concentration of monocytes in the blood (200–800 cells per μL). The initial monocyte adhesion after 8 h under TNF-α and LDL stimulation was significantly higher than the control group (no TNF-α stimulation). A p value of <0.01 was recorded in all time points up to 1 h, and an almost 3-fold increase was observed in monocyte adhesion (Fig. 6A). The time-lapse fluorescence images showed a gradual increase in the monocyte adhesion on the SVEC-10 monolayer over time (Fig. 6D and E). We conducted a control experiment without LDL and TNF-α stimulation. In brief, after forming the endothelial monolayer in the top channel, monocytes were introduced at a flow rate of 1000 s^{-1} for one hour without any previous stimulation. No monocyte adhesion was observed on the endothelial monolayer in the absence of LDL and TNF-α stimulation (Fig. S3†), highlighting the necessity of these stimuli for inducing monocyte–endothelial interactions. Next, we observed endothelial transmigration and the potential for foam cell formation in the subendothelial intima. Within 15 min of infusion through the top channel, monocytes began transmigrating into the subendothelial intima layer. Fig. S4† showed transmigrated monocytes in the intimal layer during monocyte infusion into the top channel, indicating a dysfunctional endothelium layer upon TNF-α stimulation. Moreover, TNF-α stimulation significantly increased the number of the transmigrated cells, and an almost 5-times increase in the number of transmigrated cells was recorded in the TNF-α treated group than the control (Fig. 6B). Most importantly, the model allowed *in vivo*-like lipid accumulation in the subendothelial layer and triggered lipid-laden foam cell conversion. The percentage of foam cell formation in the total transmigrated cells was significantly higher ($p < 0.01$) in the TNF-α stimulated group than control, and an almost 2-fold increase in the percentage of foam cells was recorded (Fig. 6C). Foam cells and monocytes differed morphologically based on lipid accumulation. Microscopic images confirmed foamy morphology in fixed cells in thin smears due to lipid deposition (red/orange droplets) in the cell cytoplasm. A distinct foamy morphology was detected upon lipid accumulation in the cell cytoplasm. In contrast, monocytes have rounded and smooth morphology with distinct bluish-purple colour without any lipid droplets in the cytoplasm, which was also supported by previous studies.[50,51] The control group showed less foam cell formation (Fig. 6F), while more foam cells were detected in the TNF-α stimulated sample in the thin smear (Fig. 6G). The zoomed images showed the distinguishable morphology between monocytes and foam cells. Giemsa staining in the device also confirmed the less monocyte transmigration in

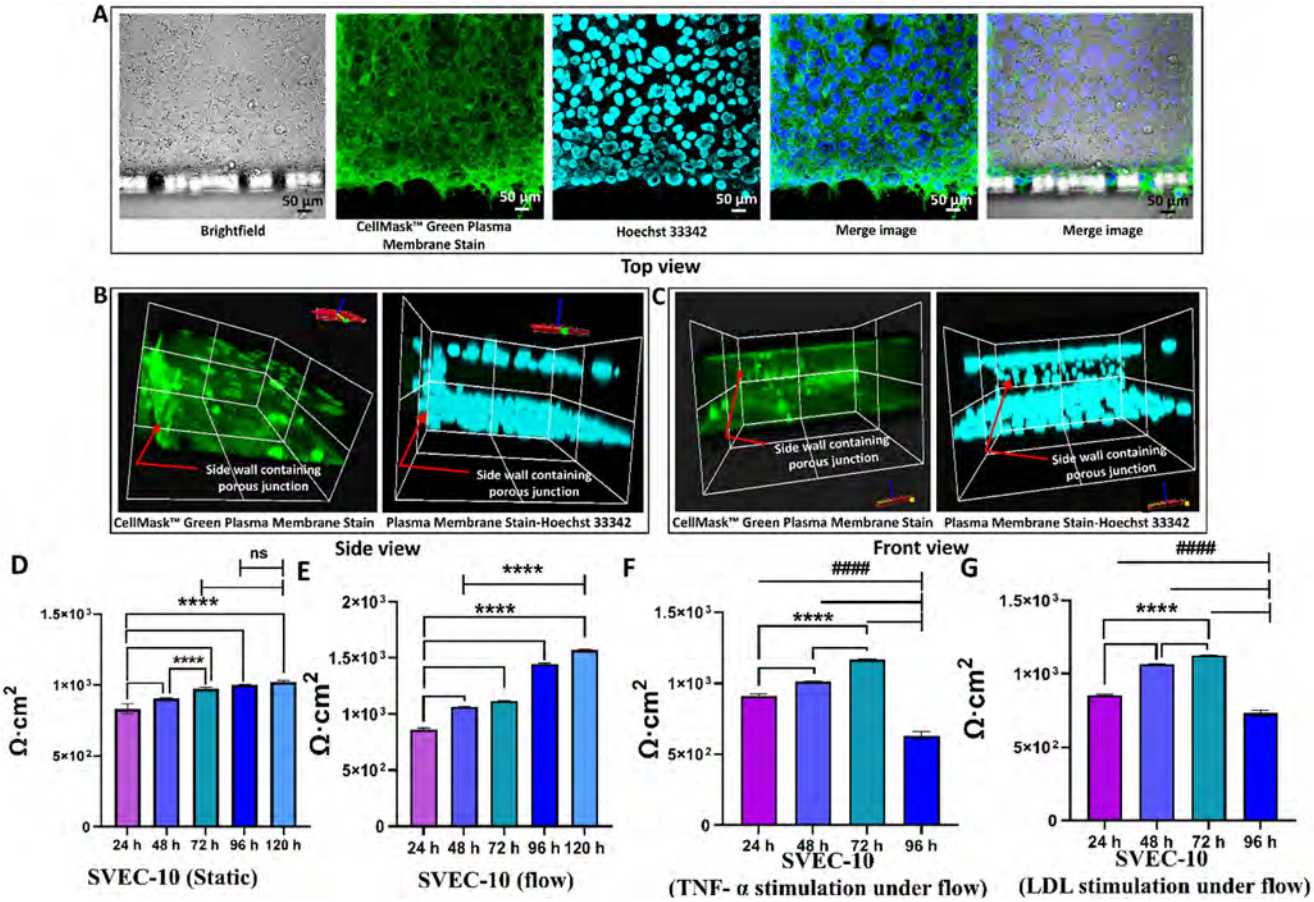

Fig. 5 Confirmation of the endothelial integrity over the porous interconnected junction between two channels. Z-Stack images were taken using a confocal microscope. (A) Top view of the side wall of the top channel containing the porous inter-junction. Plasma membrane staining (green) and nucleus staining (blue) confirm the confluent monolayer of SVEC-10 on the side wall of the bottom channel. The merged image with the brightfield view clearly showed the compact distribution of the cells in the porous area and formed a tight endothelial barrier over the porous junction area. The 3D-reconstructed images of the (B) side view and (C) front view of the top channel. The 3D reconstruction of the Z-stack images confirmed the endothelial barrier on the porous junction and a hollow lumen formation in the top channel. The red arrows depict the position of the side wall containing the porous junction. Transendothelial electrical resistance (TEER) values of untreated SVEC-10 monolayer under static condition (D), untreated SVEC-10 monolayer under the flow condition (E), TNF-α (10 ng mL^{-1}) stimulation (F), and LDL (25 μg mL^{-1}) stimulation (G) for 24 h on SVEC-10 monolayer under the flow condition. Values are mean ± SD, n = 4. ****$p < 0.0001$, and $^{\#\#\#\#}p < 0.0001$ are the increase and decrease in TEER value among different time points, respectively.

control (Fig. 6H), while a significant number of transmigrated monocytes were observed in the TNF-α stimulated group (Fig. 6I).

3.4. Inhibitory effect of aspirin in monocyte adhesion and transmigration

Aspirin, a known anti-inflammatory drug, proved beneficial in inhibiting early atherosclerosis pathogenicity by reducing initial monocyte adhesion.[52,53] To validate our device as a drug testing tool, we treated our model with different doses of aspirin (50 and 100 μM) along with TNF-α and LDL stimulation to evaluate the aspirin's inhibitory function in our device. The number of initial adherent monocytes on the SVEC-10 monolayer (top channel) was calculated, and a significant reduction in the adherent cell number was detected in both doses of aspirin compared to the TNF-α and LDL-stimulated group (Fig. 7A). However, there was no comparable difference between the doses. The total number of the transmigrated cells in the subendothelial layer (bottom channel) was counted after 24 h incubation under an arterial shear rate. The data were normalised to the negative control (no aspirin or TNF-α stimulation). A significant increase ($P < 0.001$) in the transmigrated cell number was recorded in the TNF-α and LDL-treated group (positive control) compared to the negative control. An almost 7.5-fold increase in the total number of transmigrated cells was calculated in the TNF-α group than the negative control. However, aspirin treatment reduced the transmigration significantly in both doses, and an approximately 3.5-fold reduction in the cell transmigration was recorded in the 100 μM aspirin-treated group compared to the positive control (Fig. 7B). A similar trend was observed in the percentage of foam cells in the total transmigrated cells. An increase in the percentage of the

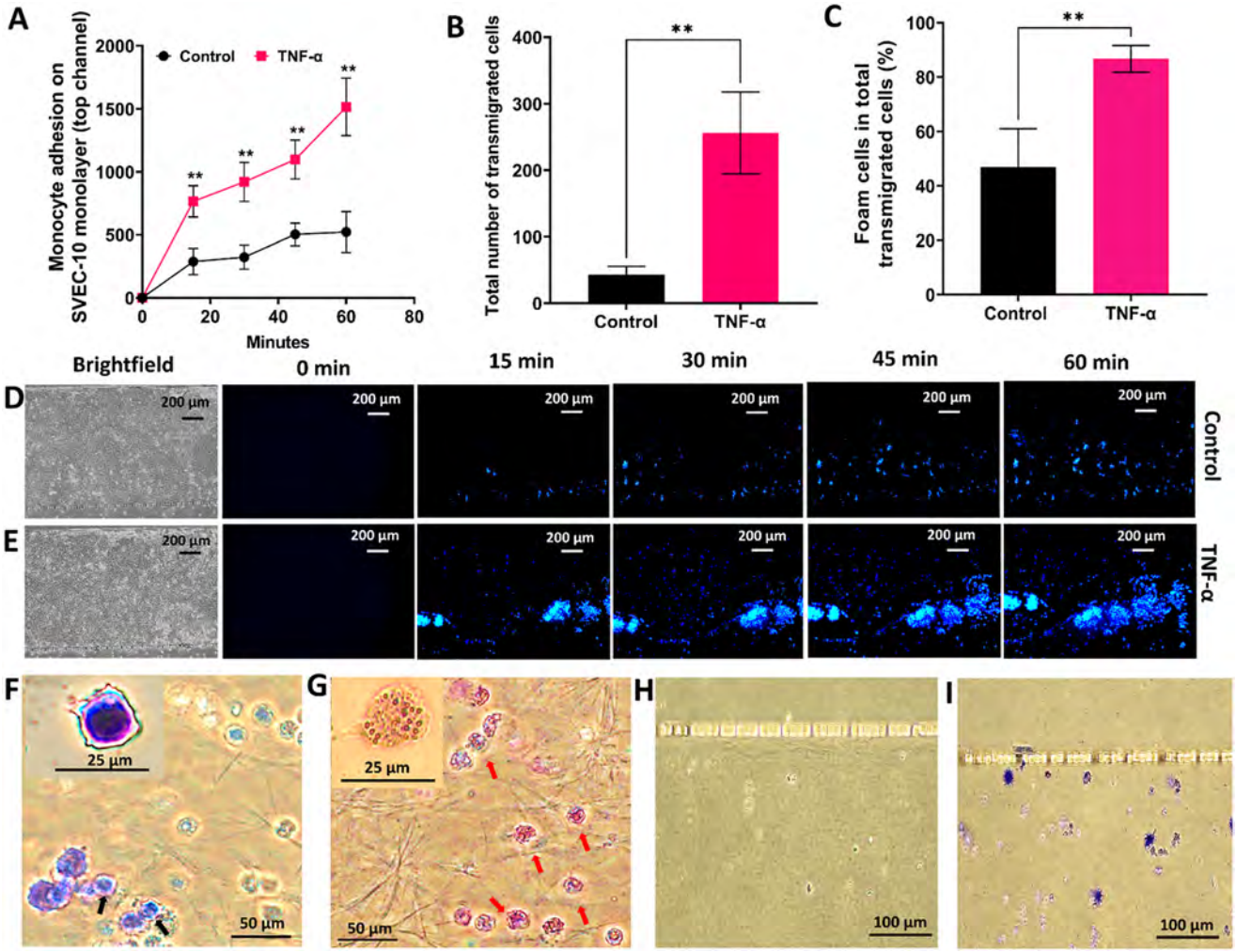

Fig. 6 Monocyte transmigration and foam cell formation in a microfluidic atherosclerosis intimal-lumen model. (A) Monocyte adhesion on the SVEC-10 monolayer in the top channel mimicking vascular lumen. The intimal-lumen model was treated with TNF-α (10 ng mL^{-1}) and LDL (25 μg mL^{-1}) at an arterial shear rate (1000 s^{-1}) before the monocyte infusion. The control group was treated only with LDL. The TNF-α group treated with TNF-α along with LDL significantly enhanced the monocyte adhesion compared to the control. (B) Total number of transmigrated cells in the subendothelial intimal layer (bottom channel) after 24 h incubation under an arterial shear rate. A significant rise in the transmigrated cell number was observed in the TNF-α stimulated group than in the control. (C) Percentage of foam cells in the total transmigrated cells in the subendothelial intimal layer. The conversion of monocytes into foam cells was significantly higher in the TNF-α stimulated group compared to the non-stimulated one. Fluorescence images of the initial adherent monocytes on the SVEC-10 monolayer (top channel) in the control group (D) and TNF-α stimulated group (E) at 1000 s^{-1} shear rate at different time points. The blue colour (Hoechst 33342) indicated adherent monocytes. A rapid increase in adherent monocytes was observed in the TNF-α stimulated group. Microscopic images of the thin smear of the transmigrated cells in the control group (F) and TNF-α stimulated group (G). The lipid droplets were visible in red/orange colour in the foam cell and provided a granular foamy morphology (red arrow). The monocytes gave a strong purple colour with apparently smooth rounded morphology (black arrow). A higher number of monocytes were detected in the control group, whereas the TNF-α stimulated group showed increased foam cell formation. Giemsa staining of the intimal layer (bottom channel) and the detection of transmigrated monocytes in the control device (H) and the TNF-α stimulated device (I). Monocytes were hardly detected in the control device, where a significant number of monocytes (purple) were detected in the intimal layer of the TNF-α stimulated device. Values are mean ± SD, $n = 3$, t-test. $^{**}p < 0.01$.

foam cell conversion was observed in the TNF-α treated group than the negative control at a p value of <0.01. On the other hand, aspirin treatment remarkably reduced the percentage of the foam cell in the total transmigrated cells in a dose-dependent manner, and both doses reduced the percentage significantly compared to the positive control. 100 μM aspirin and negative control groups had almost similar foam cell percentages (Fig. 7C). The fluorescence images further confirmed the reduced monocyte adhesion in the aspirin-treated groups than the TNF-α stimulated one (Fig. 7D–F). The blue colour from the nucleus staining indicated the adherent monocytes on the SVEC-10 monolayer in the top channel.

4. Discussion

An interplay between vascular and inflammatory cells is crucial in atherosclerosis pathogenicity. The adhesion of

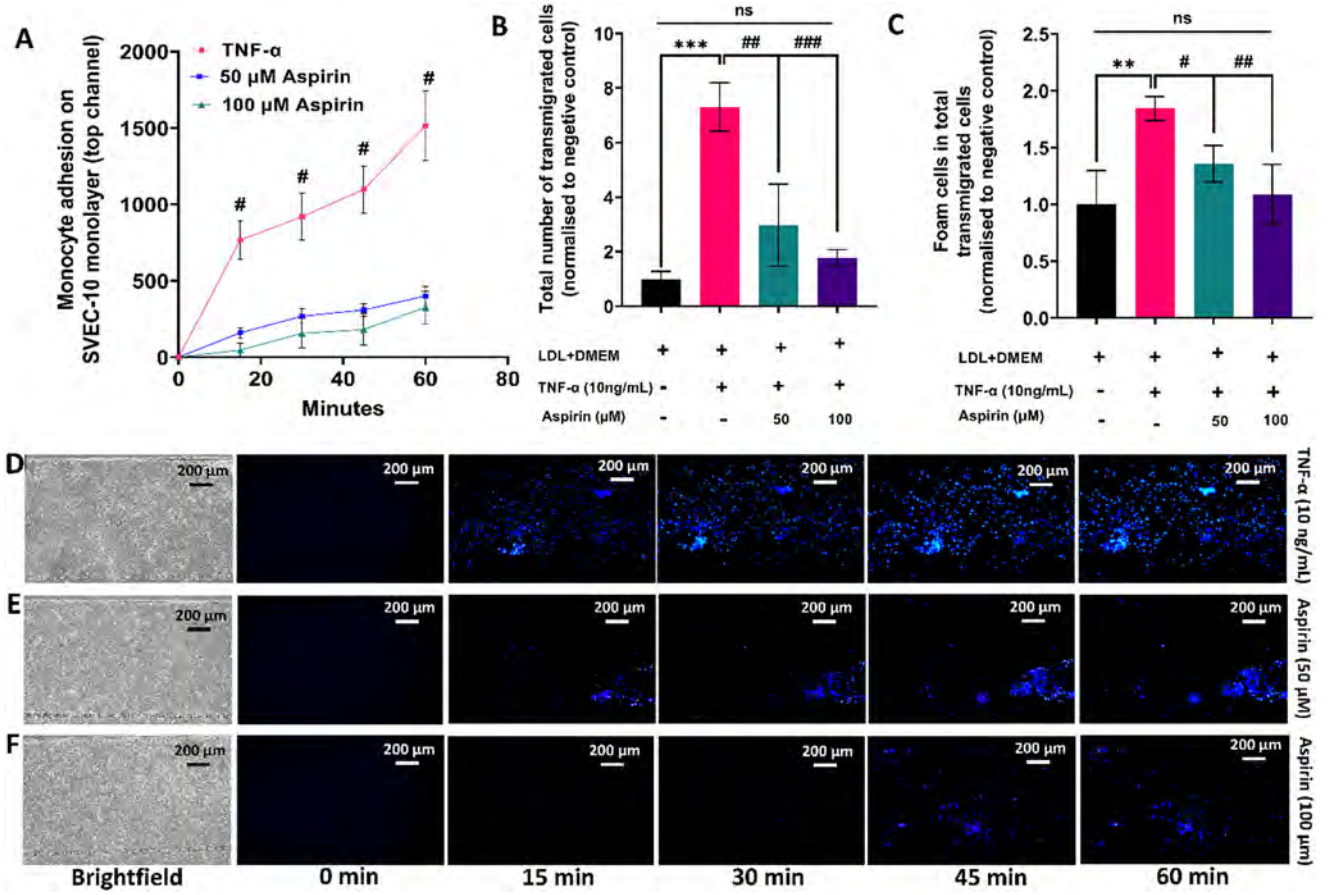

Fig. 7 Inhibitory effect of aspirin in monocyte adhesion and transmigration in the microfluidic intimal-lumen model. (A) Monocyte adhesion on the SVEC-10 monolayer in different groups. The intimal-lumen model was treated with aspirin along with TNF-α (10 ng mL^{-1}) and LDL (25 μg mL^{-1}) at an arterial shear rate (1000 s^{-1}) before monocyte infusion. The positive control group was treated only with TNF-α and LDL. Aspirin treatment in both doses significantly reduced the initial monocyte adhesion, while no comparable difference between doses was detected. (B) Comparison of the total number of transmigrated monocytes among aspirin-treated groups and the positive control. The value was normalised to the negative control (no aspirin and no TNF-α treatment). A significant reduction in the total transmigrated cell was found in the aspirin-treated groups compared to the positive control, while no significant difference was detected between the two doses and the negative control. (C) Conversion of monocytes into foam cells in the total transmigrated cells in different treated groups. The aspirin-treated groups showed a significant reduction in foam cell conversion. There were no significant differences in the aspirin-treated groups and the negative control. The value was normalised to the negative control (no aspirin and no TNF-α treatment). Fluorescence images of the initial adherent monocytes on the SVEC-10 monolayer (top channel) in the positive control (D), 50 μM aspirin-treated (E), and 100 μM aspirin-treated (F) groups at an arterial shear rate (1000 s^{-1}) in different time points. The blue colour (Hoechst 33342) indicated adherent monocytes. A reduced number of adherent monocytes was observed in the aspirin-treated groups. Values are mean ± SD, n = 3, one-way ANOVA. *Increase compared to the negative control, **$p < 0.01$, ***$p < 0.001$. #Decrease compared to the positive control, #$p < 0.05$, ##$p < 0.01$, ###$p < 0.001$.

monocytes on dysfunctional endothelial cells, followed by their transmigration into the subendothelial intima, is considered as a hallmark of atherosclerosis. The role of dysfunctional endothelial in monocyte recruitment during the early stage of atherosclerosis is well-known, but current studies suggest the process is reversible and might not be the only factor linked to the clinical consequence of atherosclerosis.[54–57] In addition to endothelium, evidence showed that vascular smooth muscle cells (VSMCs) also play a vital role in atherosclerosis progression. The effect of vascular smooth muscle (VSMCs) in arterial intimal thickening is well known. The migration of VSMCs to the intima in animal models is mediated by platelet-derived growth factors (PDGF), fibroblast growth factors (bFGF), and transforming growth factors (TGFβ).[58] When VSMCs are present in the intimal, they secrete negatively-charged proteoglycans that bind positively-charged apolipoprotein B (apoB) on atherogenic lipoproteins. This process promotes lipid retention in the subendothelial space prior to any significant monocyte/macrophage infiltration in the intima.[59,60] Moreover, intimal VSMCs interact with the transmigrated monocytes, contributing to monocyte retention and function within the vasculature, resulting in foam cell formation.[61] Also, the coculture of human VSMCs with monocytes could increase CD36 scavenger receptor expression and ox-LDL uptake *in vitro*.[60] Suggesting evidence influenced us to use the coculture of both vascular endothelial cells, and smooth muscle cells in this study. This

study focused on developing a 3D model of early atherosclerosis to mimic *in vivo*-like monocyte transmigration and foam cell formation in a microfluidic platform.

The vascular intimal layer was achieved by collagen-embedded murine smooth muscle cells, lining with murine endothelial forming a vascular lumen in the microfluidic device. The MOVAS embedded in the collagen construct in the bottom channel of the device showed good viability in the selected collagen concentration (3.5 mg mL^{-1}) and maintained viability above 60% in 5 days of incubation. The lipid depletion from the death of smooth muscle cells further contributes to atherosclerosis intimal thickening.[62] The confocal imaging confirmed the formation of the vessel lumen in the top channel of the device, and a hollow lumen formation was observed in the 3D-reconstructed images. The main advantage of our model was inducing foam cell formation in the coordination of native LDL and an arterial shear rate. We checked the model validity as a simple alternative to *in vivo* models to replicate the early stage of atherosclerosis pathogenicity. After activation of the endothelium monolayer in the top channel with TNF-α and native LDL, monocytes circulated through the top channel were found to adhere to the activated endothelium and transmigrate through the porous junction into the intima channel. The initial monocyte adhesion was significantly higher in the TNF-α and LDL-activated groups than those in the LDL-treated group. On the other hand, the circulatory native LDL used in this study might transfuse through the porous junction and retain in the intimal layer allowing *in vivo*-like oxidation and accumulation by monocytes for foam cell formation.[62,63]

Conversion into lipid-laden foam cell formation of the transmigrated monocytes plays a key pathological role in the atherosclerotic lesion.[64] There is indeed a requirement for developing a physiologically relevant model that can replicate the human pathophysiology for understanding the disease mechanism and testing therapeutic molecules. Activating the endothelial monolayer with TNF-α and LDL in our model triggered significant transendothelial monocyte transmigration and foam cell conversion under an arterial shear rate. Interestingly, the results were directly associated with the pathophysiology of atherosclerosis in the human body, which involves endothelial dysfunction, monocyte recruitment, and subsequent transmigration.[2,65–67] The existing *in vivo* models, including small and big animals, mostly create severe dyslipidaemia to induce an inflammatory environment for the cells and promote rapid monocyte recruitment to initiate early events of atherosclerosis.[68,69] These animal models undergo multiple genetic modifications to generate atherosclerosis, which makes them highly expensive and time-consuming. For example, Zhao *et al.*[70] developed an LDLr KO (low-density lipoprotein receptor knockout) mice reconstituted with ABCA1/SR-BI (ATP-binding cassette transporter 1/scavenger receptor class B type I) double knockout bone marrow model for macrophage-derived foam cell formation atherosclerotic lesion development. Wang *et al.*[71] used USP9X-deficient mice and showed increased infiltration of macrophage infiltration and lipid deposition compared to the control mice (apolipoprotein E-KO).

Aspirin was chosen to demonstrate the potential application of our microfluidic model as a drug-testing tool. Aspirin, a known anti-inflammatory drug, is suggested to reduce early atherosclerosis pathogenesis by decreasing the circulating levels and vascular formation of soluble intercellular molecule-1, monocyte chemoattractant protein-1 (MCP-1), TNF-α, interleukin-12p40, without affecting lipid levels in LDL-receptor-deficient mice fed with a high-fat diet compared with control mice.[72] Aspirin administration has also been reported to reduce the development and progression of atherosclerosis in hyperlipidemic mice.[73] Our model showed a significant reduction in monocyte recruitment and transmigration by adding small doses of aspirin (50 and 100 μM) compared to the positive control group (TNF-α and LDL). Moreover, the foam cell conversion in the total transmigrated cells was significantly reduced in the aspirin-treated groups in our model. Many studies supported the finding. A study reported that aspirin inhibited TNF-alpha (10 ng ml^{-1})-induced MCP-1 and IL(interleukin)-8 expression in human umbilical vein endothelial cells (HUVECs).[74] Aspirin at a dose of 10 μg mL^{-1} (~50 μM) significantly inhibited the release of MCP-1 by 29.1% and IL-8 by 26.9% compared to the TNF-stimulated group. The direct effect on monocyte adhesion was checked, and aspirin treatment inhibited the initial adhesion by 13.4% while inhibiting transmigration by 89.1% compared to the TNF-α treated group. Similar findings were suggested by Weber *et al.*[53] They showed that aspirin suppressed TNF-α-induced NF-kB activation in endothelial cells to inhibit expressions of vascular cell adhesion molecule-1 (VCAM-1) and E-selectin. Aspirin's dose-dependent inhibition of TNF-induced NF-κB mobilization was achieved at concentrations ranging from 1 to 10 mM. As a functional consequence, the adhesion of U937 monocytes to TNF-stimulated HUVECs was markedly reduced by aspirin due to suppression of VCAM-1 and E-selectin upregulation. Furthermore, cell adhesion molecule expression on monocytes after activation was significantly reduced by aspirin, which might explain the reduced migratory ability.[75]

Overall, we successfully developed a microfluidic intimal-lumen model for replicating the early event of atherosclerosis. The best part of our model was the incorporation of the 3D physiological microenvironment, including cell–cell, cell–matrix interaction with continuous hemodynamic modulation to replicate the native physiology. In the dual-interconnected microchannels, vascular coculture was developed under physiological shear rate and *in vivo*-like monocyte recruitment on the inflamed endothelial was achieved. The model also used native LDL, retained the transmigrated monocytes in the subendothelial intimal space, and converted the transmigrated monocyte into foam cells under a physiological shear rate. We utilised the model

to test the anti-inflammatory effect of aspirin and observed its sensitivity in treating early atherosclerosis events. This simple but robust model could be used as an excellent alternative to the genetically modified complex animal models to study the different aspects of early atherosclerosis development and could be employed to test therapeutic compounds.

5. Limitation and future direction

Despite the promising findings achieved from the current model, several limitations need to be addressed in the future. The present study did not quantify the LDL diffusion and oxidation in the subendothelial space, which is crucial for foam cell formation. The confirmation could be done by using fluorescence-tagged LDL in future. Moreover, we did not check the phenotypic alteration of the MOVAS in the intimal layer. VSMCs in the atherosclerotic intima reduced contractility and converted into synthetic phenotype. We also did not consider the MOVAS-derived foam cell formation in our model. The VSMC-derived and macrophage-derived foam cell percentages are important parameters for evaluating our model's physiological relevancy. Another drawback of the current study is the short-term coculture. Atherosclerosis intimal thickening is a slow process and requires long-term incubation. Our current study period was only 4 days, which might not fully replicate the intimal thickening. In the future, the model could be used with fluorescence dye to visualize the different steps in converting monocytes to foam cells in real time. The expression level of adhesion molecules in the endothelial layer should be measured to study the biochemical interaction and mechanism behind monocyte recruitment. Moreover, we would employ the long-term coculture to initiate extracellular matrix production from the vascular cells for intimal thickening. Changes in cell–matrix stiffness can be measured to assess the capability of the device to form the plaque. In future studies, we will incorporate different vessel geometry, including vessel stenosis to mimic the vessel complexities in assessing atherosclerosis risk in our developed platform.

Data availability

Data is available upon request.

Conflicts of interest

There are no conflicts to declare.

Acknowledgements

This work is funded by National Health and Medical Research Council (HTT: APP1037310, APP1182347, APP2002827) and Heart Foundation (HTT: 102761). The authors would like to acknowledge the Australian National Fabrication Facility (Queensland Node) for access to key items of equipment.

References

1 A. L. Olivares, M. A. González Ballester and J. Noailly, *Bioinformatics*, 2016, **32**, 3798–3806.
2 V. Mallika, B. Goswami and M. Rajappa, *Angiology*, 2007, **58**, 513–522.
3 Y. Wu, G. Cowin, S. S. Moonshi, H. D. N. Tran, N. A. Fithri, A. K. Whittaker, R. Zhang and H. T. Ta, *Mater. Sci. Eng., C*, 2021, **131**, 112477.
4 B. Perera, Y. Wu, N. T. Nguyen and H. T. Ta, *Mater. Today Bio*, 2023, **22**, 100767.
5 K. X. Vazquez-Prada, S. S. Moonshi, Z. P. Xu and H. T. Ta, *Appl. Mater. Today*, 2023, **35**, 101967.
6 F. Akther, H. D. Tran, J. Zhang, N.-T. Nguyen and H. T. Ta, in *Nanotechnology for Hematology, Blood Transfusion, and Artificial Blood*, Elsevier, 2022, pp. 237–264.
7 M. Rafieian-Kopaei, M. Setorki, M. Doudi, A. Baradaran and H. Nasri, *Int. J. Prev. Med.*, 2014, **5**, 927–946.
8 J. R. Pickett, Y. Wu, L. F. Zacchi and H. T. Ta, *Cardiovasc. Res.*, 2023, **119**, 2278–2293.
9 F. Akther, J. Zhang, H. D. N. Tran, H. Fallahi, H. Adelnia, H. P. Phan, N. T. Nguyen and H. T. Ta, *Adv. Biol.*, 2022, **6**, e2101316.
10 P. Libby, *Arterioscler., Thromb., Vasc. Biol.*, 2012, **32**, 2045–2051.
11 F. Pappalardo, S. Musumeci and S. Motta, *Bioinformatics*, 2008, **24**, 1715–1721.
12 M. Aziz and K. S. Yadav, *Med. Clin. Rev.*, 2016, **2**, 22.
13 F. Akther, D. Sajin, S. S. Moonshi, Y. Wu, K. X. Vazquez-Prada and H. T. Ta, *Adv. Biol.*, 2024, **8**, e2300463.
14 R. Piga, Y. Naito, S. Kokura, O. Handa and T. Yoshikawa, *Atherosclerosis*, 2007, **193**, 328–334.
15 M. Inoue, T. Ishida, T. Yasuda, R. Toh, T. Hara, H. M. Cangara, Y. Rikitake, K. Taira, L. Sun, R. K. Kundu, T. Quertermous and K. Hirata, *Microvasc. Res.*, 2010, **80**, 179–187.
16 S. L. Ullevig, Q. Zhao, D. Zamora and R. Asmis, *Atherosclerosis*, 2011, **219**, 409–416.
17 T. Keiper, N. Al-Fakhri, E. Chavakis, A. N. Athanasopoulos, B. Isermann, S. Herzog, R. Saffrich, K. Hersemeyer, R. M. Bohle, J. Haendeler, K. T. Preissner, S. Santoso and T. Chavakis, *FASEB J.*, 2005, **19**, 2078–2080.
18 M. Klouche, A. E. May, M. Hemmes, M. Meßner, S. M. Kanse, K. T. Preissner and S. Bhakdi, *Arterioscler., Thromb., Vasc. Biol.*, 1999, **19**, 784–793.
19 J. M. Murphy, K. Jeong, Y. A. R. Rodriguez, J. H. Kim, E. E. Ahn and S. S. Lim, *Sci. Rep.*, 2019, **9**, 7617.
20 S. Ramachandran, A. Vinitha and C. C. Kartha, *Cardiovasc. Diabetol.*, 2016, **15**, 152.
21 A. Mallone, C. Stenger, A. Von Eckardstein, S. P. Hoerstrup and B. Weber, *Biomaterials*, 2018, **150**, 49–59.
22 J. Chen, X. Zhang, R. Millican, T. Lynd, M. Gangasani, S. Malhotra, J. Sherwood, P. T. Hwang, Y. Cho, B. C. Brott, G. Qin, H. Jo, Y. S. Yoon and H. W. Jun, *Front. Cardiovasc. Med.*, 2021, **8**, 790529.

23 S. Oppi, T. F. Lüscher and S. Stein, *Front. Cardiovasc. Med.*, 2019, **6**, 46.
24 M. Gao, G. Xin, X. Qiu, Y. Wang and G. Liu, *J. Biomed. Res.*, 2016, **31**, 47–55.
25 J. Fan, S. Kitajima, T. Watanabe, J. Xu, J. Zhang, E. Liu and Y. E. Chen, *Pharmacol. Ther.*, 2015, **146**, 104–119.
26 J. Shim, R. Al-Mashhadi, C. Sørensen and J. Bentzon, *J. Pathol.*, 2016, **238**, 257–266.
27 G. S. Getz and C. A. Reardon, *Arterioscler., Thromb., Vasc. Biol.*, 2012, **32**, 1104–1115.
28 A. Gisterå, D. F. J. Ketelhuth, S. G. Malin and G. K. Hansson, *Circ. Res.*, 2022, **130**, 1869–1887.
29 J. W. Knowles and N. Maeda, *Arterioscler., Thromb., Vasc. Biol.*, 2000, **20**, 2336–2345.
30 W. Zheng, R. Huang, B. Jiang, Y. Zhao, W. Zhang and X. Jiang, *Small*, 2016, **12**, 2022–2034.
31 C. Su, N. V. Menon, X. Xu, Y. R. Teo, H. Cao, R. Dalan, C. Y. Tay and H. W. Hou, *Lab Chip*, 2021, **21**, 2359–2371.
32 W. Zheng, R. Huang, B. Jiang, Y. Zhao, W. Zhang and X. Jiang, *Small*, 2016, **12**, 2022–2034.
33 X. Zhang, M. Bishawi, G. Zhang, V. Prasad, E. Salmon, J. J. Breithaupt, Q. Zhang and G. A. Truskey, *Nat. Commun.*, 2020, **11**, 5426.
34 J. H. Lee, Z. Chen, S. He, J. Zhou, A. Tsai, G. Truskey and K. W. Leong, *Adv. Biol.*, 2021, **5**, e2000428.
35 R. Maringanti, C. G. M. van Dijk, E. M. Meijer, M. M. Brandt, M. Li, V. P. C. Tiggeloven, M. M. Krebber, I. Chrifi, D. J. Duncker, M. C. Verhaar and C. Cheng, *Arterioscler., Thromb., Vasc. Biol.*, 2024, **44**, 2453–2472.
36 N. V. Menon, H. M. Tay, K. T. Pang, R. Dalan, S. C. Wong, X. Wang, K. H. H. Li and H. W. Hou, *APL Bioeng.*, 2018, **2**, 016103.
37 Y. Shin, S. Lim, J. Kim, J. S. Jeon, H. Yoo and B. Gweon, *Lab Chip*, 2019, **19**, 3664–3677.
38 R. Das, S. Ganapathy, G. H. Mahabeleshwar, C. Drumm, M. Febbraio, M. K. Jain and E. F. Plow, *Circulation*, 2013, **127**, 1209–1218.
39 X. Gu, S. Xie, D. Hong and Y. Ding, *Sci. Rep.*, 2019, **9**, 7461.
40 F. Akther, J. Zhang, H. D. N. Tran, H. Fallahi, H. Adelnia, H. P. Phan, N. T. Nguyen and H. T. Ta, *Adv. Biol.*, 2022, e2101316, DOI: **10.1002/adbi.202101316**.
41 F. Akther, H. Fallahi, J. Zhang, N. T. Nguyen and H. T. Ta, *Lab Chip*, 2024, **24**, 2927–2943.
42 A. Milutinović, D. Šuput and R. Zorc-Pleskovič, *Bosnian J. Basic Med. Sci.*, 2020, **20**, 21–30.
43 Y. Nakashima, T. N. Wight and K. Sueishi, *Cardiovasc. Res.*, 2008, **79**, 14–23.
44 F. Akther, P. Little, Z. Li, N.-T. Nguyen and H. T. Ta, *RSC Adv.*, 2020, **10**, 43682–43703.
45 M. A. Panteleev, N. Korin, K. D. Reesink, D. L. Bark, J. M. E. M. Cosemans, E. E. Gardiner and P. H. Mangin, *J. Thromb. Haemostasis*, 2021, **19**, 588–595.
46 C. Poon, *J. Mech. Behav. Biomed. Mater.*, 2022, **126**, 105024.
47 M. C. Ceccarelli, M. C. Lefevre, A. Marino, F. Pignatelli, K. Krukiewicz, M. Battaglini and G. Ciofani, *Lab Chip*, 2024, **24**, 5085–5100.
48 F. Akther, S. B. Yakob, N.-T. Nguyen and H. T. Ta, *Biosensors*, 2020, **10**, 182.
49 D. W. Morel, J. R. Hessler and G. M. Chisolm, *J. Lipid Res.*, 1983, **24**, 1070–1076.
50 T. A. Angelovich, M. D. Y. Shi, J. Zhou, A. Maisa, A. C. Hearps and A. Jaworowski, *Exp. Gerontol.*, 2016, **80**, 17–26.
51 T. A. Angelovich, A. C. Hearps, A. Maisa, T. Kelesidis and A. Jaworowski, *J. Visualized Exp.*, 2017, **2017**, e56293.
52 S. Husain, N. P. Andrews, D. Mulcahy, J. A. Panza and A. A. Quyyumi, *Circulation*, 1998, **97**, 716–720.
53 C. Weber, W. Erl, A. Pietsch and P. C. Weber, *Circulation*, 1995, **91**, 1914–1917.
54 R. Ross, *Nature*, 1993, **362**, 801–809.
55 C. K. Glass and J. L. Witztum, *Cell*, 2001, **104**, 503–516.
56 A. J. Lusis, *Nature*, 2000, **407**, 233–241.
57 H. Adelnia, S. S. Moonshi, Y. Wu, A. C. Bulmer, R. McKinnon, J. W. Fastier-Wooller, I. Blakey and H. T. Ta, *ACS Nano*, 2023, **17**, 18775–18791.
58 M. O. J. Grootaert, M. Moulis, L. Roth, W. Martinet, C. Vindis, M. R. Bennett and G. R. Y. De Meyer, *Cardiovasc. Res.*, 2018, **114**, 622–634.
59 P. Xiang, V. Blanchard and G. A. Francis, *Front. Physiol.*, 2022, **13**, 921597.
60 Y. Nakashima, H. Fujii, S. Sumiyoshi, T. N. Wight and K. Sueishi, *Arterioscler., Thromb., Vasc. Biol.*, 2007, **27**, 1159–1165.
61 Q. Cai, L. Lanting and R. Natarajan, *Arterioscler., Thromb., Vasc. Biol.*, 2004, **24**, 2263–2270.
62 J. L. Harman and H. F. Jørgensen, *Br. J. Pharmacol.*, 2019, **176**, 3741–3753.
63 M. Liu, S. Samant, C. H. Vasa, R. M. Pedrigi, U. M. Oguz, S. Ryu, T. Wei, D. R. Anderson, D. K. Agrawal and Y. S. Chatzizisis, *PLoS One*, 2023, **18**, e0280385.
64 C. L. V. Westhorpe, E. M. Dufour, A. Maisa, A. Jaworowski, S. M. Crowe and W. A. Muller, *Exp. Mol. Pathol.*, 2012, **93**, 220–226.
65 S. C. Bergheanu, M. C. Bodde and J. W. Jukema, *Neth. Heart J.*, 2017, **25**, 231–242.
66 S. Jebari-Benslaiman, U. Galicia-García, A. Larrea-Sebal, J. R. Olaetxea, I. Alloza, K. Vandenbroeck, A. Benito-Vicente and C. Martín, *Int. J. Mol. Sci.*, 2022, **23**, 3346.
67 K. Sakakura, M. Nakano, F. Otsuka, E. Ladich, F. D. Kolodgie and R. Virmani, *Heart, Lung Circ.*, 2013, **22**, 399–411.
68 F. K. Swirski, M. J. Pittet, M. F. Kircher, E. Aikawa, F. A. Jaffer, P. Libby and R. Weissleder, *Proc. Natl. Acad. Sci. U. S. A.*, 2006, **103**, 10340–10345.
69 F. K. Swirski, P. Libby, E. Aikawa, P. Alcaide, F. W. Luscinskas, R. Weissleder and M. J. Pittet, *J. Clin. Invest.*, 2007, **117**, 195–205.
70 Y. Zhao, M. Pennings, R. B. Hildebrand, D. Ye, L. Calpe-Berdiel, R. Out, M. Kjerrulf, E. Hurt-Camejo, A. K. Groen, M.

Hoekstra, W. Jessup, G. Chimini, T. J. C. Van Berkel and M. Van Eck, *Circ. Res.*, 2010, **107**, e20–e31.
71 B. Wang, X. Tang, L. Yao, Y. Wang, Z. Chen, M. Li, N. Wu, D. Wu, X. Dai, H. Jiang and D. Ai, *J. Clin. Invest.*, 2022, **132**, e154217.
72 T. Cyrus, S. Sung, L. Zhao, C. D. Funk, S. Tang and D. Praticò, *Circulation*, 2002, **106**, 1282–1287.
73 T. Cyrus, Y. Yao, L. X. Tung and D. Praticò, *Atherosclerosis*, 2006, **184**, 8–14.
74 Y. Y. Yang, C. J. Hu, S. M. Chang, T. Y. Tai and S. J. Leu, *Atherosclerosis*, 2004, **174**, 207–213.
75 I. E. Hoefer, S. Grundmann, S. Schirmer, N. van Royen, B. Meder, C. Bode, J. J. Piek and I. R. Buschmann, *J. Am. Coll. Cardiol.*, 2005, **46**, 994–1001.

Supplementary Information (SI) for Lab on a Chip.

Supplementary Information for

An intimal-lumen model in a microfluidic device: Potential platform for atherosclerosis-related studies

Method:

S1. Reynold number calculation:

The formula for the Reynold number is as below:

$Re=\rho v D_h/\mu$

Where:

ρ = fluid density =1000 kg/m^3

v = fluid velocity

D_h = hydraulic diameter of the channel

μ = dynamic viscosity of the fluid = 0.964×10−3 Pa.s

For a rectangular channel, the hydraulic diameter is given by:

$$D_h=\frac{2\,w\,h}{w+h}$$

Where, w=1 mm=0.1 cm, and h=100 μm=0.01 cm

So, D_h= 0.1818 cm

To calculate the velocity, we use the flow rate Q and the cross-sectional area A:

$v=Q/A$

Where, Q=100μL/min = 1.667×10−3cm^3/s, and A=w·h=0.1cm×0.01cm=0.001cm^2

Now, calculate the velocity:

$v=1.667\times10^{-3}/0.001=1.667$ cm/s

Now we can plug the values into the Reynolds number formula:

$Re=\rho v D_h/\mu$

Substituting the values:

$Re = 1 \times 1.667 \times 0.01818 / 0.964 \times 10^{-2} = 0.0303 / 0.00964$

$Re \approx 3.144$

S2. Measurement of oxidized low-density lipoprotein (ox-LDL)

Low-density lipoprotein (LDL) concentration was measured using the Micro BCA™ Protein Assay Kit (ThermoFisher Scientific, 23235), and oxidized low-density lipoprotein (ox-LDL) was quantified using a Lipid Peroxidation (MDA) Assay Kit (ab118970), following the manufacturer's protocol. Briefly, 20 µL of LDL stock (6.53 mg/ml) were gently mixed with 500 µL of 42 mM H_2SO_4, and 125 µL of phosphotungstic acid solution was added to precipitate lipids while minimizing protein contamination. After vortexing, the mixture was incubated at room temperature for 5 minutes and centrifuged at 13,000 × g for 3 minutes to collect the lipid pellet. The pellet was resuspended on ice with 100 µL of double-distilled water (ddH_2O) containing 2 µL of 100× butylated hydroxytoluene (BHT), adjusting the final volume to 200 µL with ddH_2O. To the resuspended lipid samples and malondialdehyde (MDA) standards, 600 µL of 2-thiobarbituric acid (TBA) solution (33.3 mg/mL) was added to 200 µL of both the standard (malondialdehyde – MDA) and samples. The mixture was incubated at 95°C for 60 minutes, then cooled to room temperature in an ice bath for 10 minutes. Subsequently, 200 µL of the reaction mixture, containing the MDA-TBA adduct, was transferred to a 96-well microplate for analysis. A standard curve was prepared using MDA concentrations of 0, 2, 4, 6, and 8 µM. Absorbance was measured immediately using a microplate reader (BMG LABTECH FLUOstar Omega) at 532 nm.

Figures:

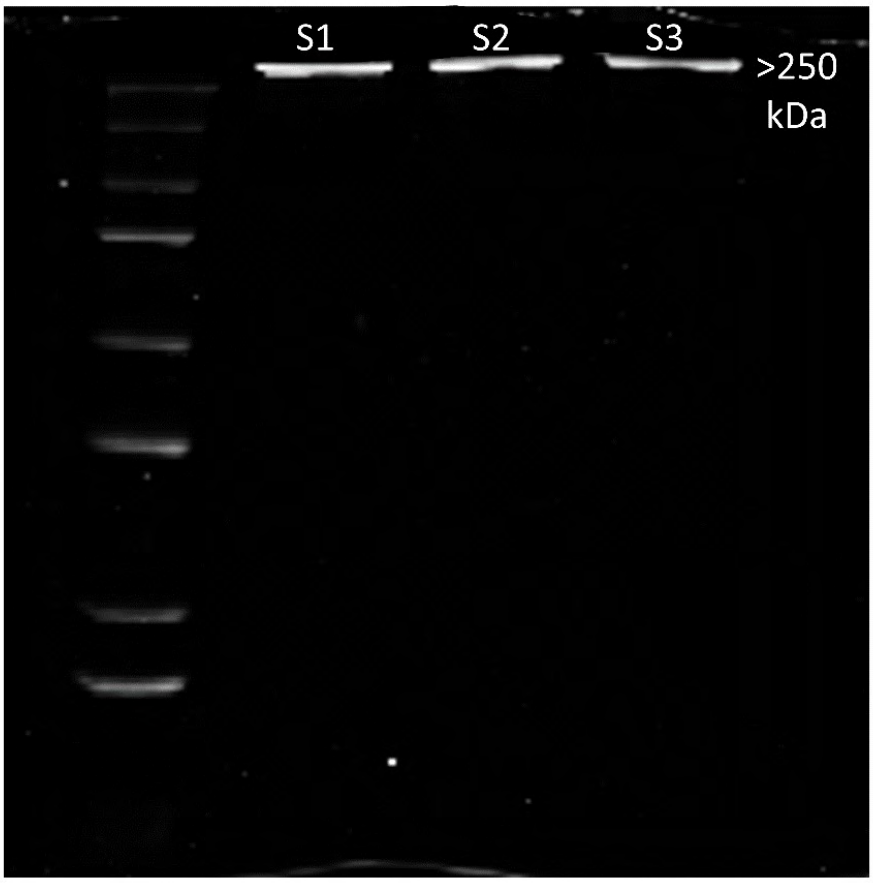

Figure S1: Confirming the low-density lipoprotein (LDL) isolation from whole blood by SDS-PAGE electrophoresis. The band achieved above 250 kDa proved successful LDL isolation. Only one band detected in the sample proved the purity. The three separate bands represented three separate isolates.

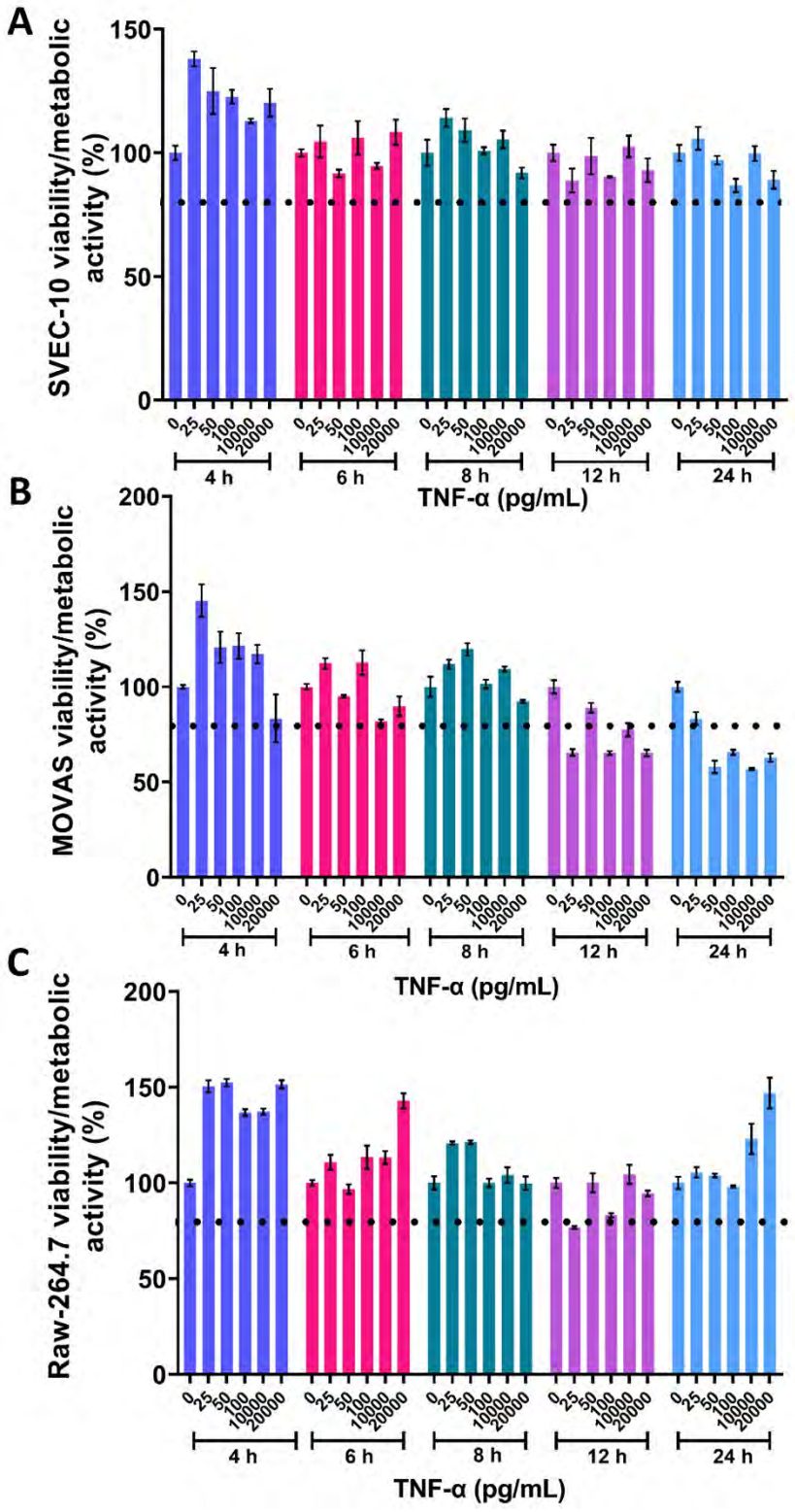

Figure S2: Cell viability/metabolic activity profiles in different TNF-α concentrations and time points. The viability/metabolic activity of **(A)** SVEC-10, **(B)** MOVAS, and **(C)** RAW 264.7. Both SVEC-10 and RAW 264.7 cells maintained good cell viability (above 80%) in all concentrations up to 24 h, while a reduction in viability/metabolic activity was observed in MOVAS after 8 h of treatment.

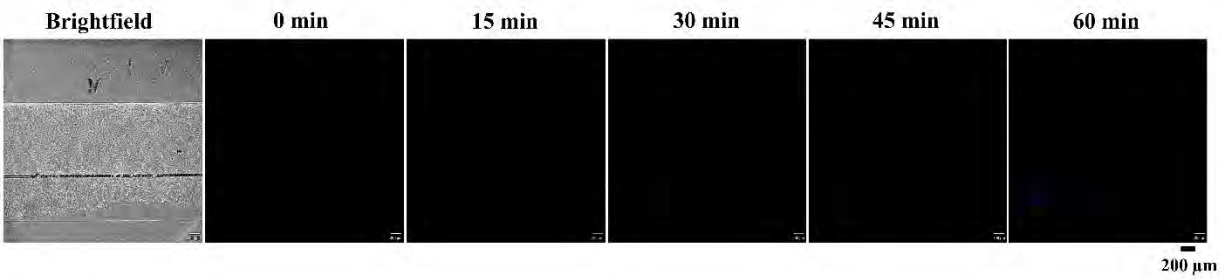

Figure S3: Monocyte adhesion on endothelial monolayer. No monocyte adhesion was observed on the endothelial monolayer in the absence of LDL and TNF-α stimulation.

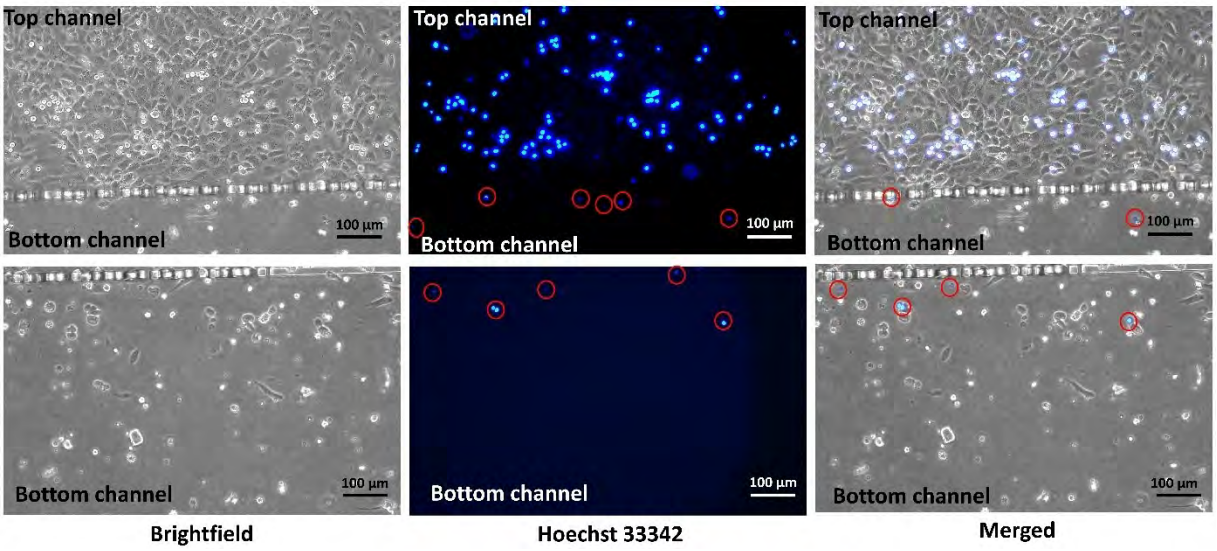

Figure S4: Subendothelial transmigration of monocyte during cell infusion through the top channel. TNF-α stimulation caused endothelial dysfunction and initiated subendothelial transmigration within 15 min of infusion. The blue colour from the nucleus staining indicated the attached monocytes in the top channel and the transmigrated monocytes in the bottom. The red circle showed the transmigrated monocytes in the fluorescence and merged images.